CHEMISTRY OF MATERIALS

Article

pubs.acs.org/cm

Catalytic "MOF-Cloth" Formed via Directed Supramolecular Assembly of UiO-66-NH_2 Crystals on Atomic Layer Deposition-Coated Textiles for Rapid Degradation of Chemical Warfare Agent Simulants

Dennis T. Lee,[†] Junjie Zhao,[†] Gregory W. Peterson,[‡] and Gregory N. Parsons*[,†]

[†]Department of Chemical & Biomolecular Engineering, North Carolina State University, 911 Partners Way, Raleigh, North Carolina 27695, United States

[‡]Edgewood Chemical Biological Center, 5183 Blackhawk Road, Aberdeen Proving Ground, Maryland 21010, United States

Supporting Information

ABSTRACT: Highly tunable metal−organic framework (MOF) materials, including, for example, UiO-66-NH_2, are known to be effective catalysts to degrade chemical warfare agents (CWAs) with half-lives near 1 min. Therefore, many researchers have been actively working on producing supported MOF materials to improve application effectiveness by using relatively slow solvothermal synthesis or repetitious stepwise layer-by-layer methods. Herein, we demonstrate a facile route to rapidly assemble presynthesized UiO-66-NH_2 crystals onto nonwoven polypropylene (PP) fibrous mats at ambient temperature. Crystal assembly is chemically directed using β-cyclodextrin (β-CD) and cetyltrimethylammonium bromide (CTAB) as surfactant assembly agents, where the agents quickly (within 5 min) self-assemble on the crystal surface and promote physically robust chemical surface attachment while simultaneously impeding solution-phase crystal agglomeration. Furthermore, we find that when the PP is preconditioned using conformal metal oxide thin films, including Al_2O_3, TiO_2, or ZnO formed via atomic layer deposition (ALD), the hydrophilic metal oxide surface further helps improve assembly uniformity and MOF mass loading, producing MOF crystal loading as high as 40 wt % and an overall BET surface area exceeding 200 $m^2/g_{(MOF+Fiber)}$. Using these surface-assembled MOFs, we observe catalytic degradation of dimethyl 4-nitrophenyl phosphate (DMNP), a CWA simulant, with a half-life of less than 5 min.

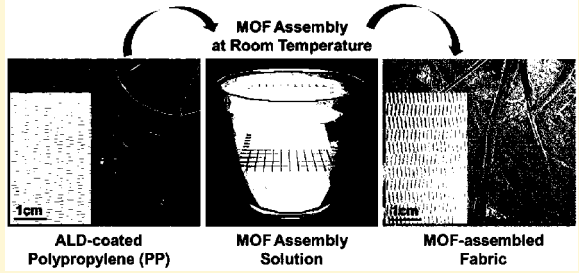

INTRODUCTION

Metal−organic frameworks (MOFs) are porous and highly crystalline materials assembled by bridging nanoscale metal ions or clusters with multifunctional organic linkers.[1] Since MOFs can exhibit tunable porous structures, exceptionally high surface area, and good chemical, hydrolytic, and thermal stability,[2] they have been explored for a range of applications, such as gas storage and separation,[3] catalysis,[4] light harvesting and energy conversion,[5] selective adsorption of anions from aqueous solutions,[6] and recently degrading chemical warfare agents (CWAs).[7,8] However, MOF batch synthesis methods often require both high reaction temperatures and long reaction time and result in powders that require further handling and processing for further applications.[9]

To overcome the problem of MOF processing, many approaches have been reported to integrate MOFs into polymeric,[10] organic−inorganic fibrous mats,[11] and polymer matrices.[12−14] To date, however, these approaches are limited to demonstrations using MOF precursor solutions to form crystals via methods including in situ solvothermal synthesis,[15,16] layer-by-layer growth,[17] counter-diffusion,[18] or microwave irradiation,[19] many of which require high temperatures or relatively long processing times. Unless care is taken to prepare the surface to promote MOF crystal nucleation,[20,21] these methods commonly lead to poor coverage of MOFs and low MOF mass fraction on the substrate. Poor surface coverage results from relatively rapid nucleation in the solution phase, thereby depleting reactants available for slower surface nucleation and growth.

Herein, we report a facile and rapid strategy for integration of MOFs onto polymeric fibrous mats at ambient temperature using solvent-suspended presynthesized MOF crystals. To demonstrate this strategy, we use UiO-66-NH_2 and provide new insight to allow direct assembly and achieve high MOF mass fraction on polypropylene (PP) nonwoven mats. We examine UiO-66-NH_2 because it is a highly stable Zr-based MOF known to be effective for catalytic destruction of organophosphorus nerve agents and related simulants, such as dimethyl 4-nitrophenyl phosphate (DMNP).[22,23] A challenge for MOF assembly on polypropylene is that the polymer surface displays only methyl groups, which cannot form covalent bonds with UiO-66-NH_2 crystals due to polar amine

Received: March 7, 2017
Revised: May 12, 2017
Published: May 12, 2017

DOI: 10.1021/acs.chemmater.7b00949
Chem. Mater. 2017, 29, 4894−4903

functional groups.[24] To promote the interaction between the MOF and the substrate, we introduced atomic layer deposition (ALD) of metal oxides to impart surface hydroxyl groups onto the inert PP.[25] A supramolecular complex comprised of β-cyclodextrin (β-CD) and cetyltrimethylammonium bromide (CTAB) was used as a self-assembly agent. The hydroxyl units on the cylindrical β-CD and cationic head groups on the linear CTAB molecules lead to a host−guest self-assembly interaction and bind to polar surfaces (including both the MOF and the modified PP) via van der Waals, electrostatic interactions, and hydrogen bonding.[26−28] The modified surfaces then readily bind to each other at room temperature, leading to dense MOF assembly on the PP. Furthermore, the β-CD and CTAB surface assembly agents work to minimize MOF crystal agglomeration in solution, thereby enabling high mass-loading, conformal coverage, and physically robust surface-attachment of UiO-66-NH_2 crystals. To the best of our knowledge, this is the first demonstration of chemical assembly of presynthesized MOF crystals with high mass loading on textiles utilizing surface assembly agents. We also substantiate that the assembled MOFs retain their functional surface area and catalytic activity and show that the PP/ALD/MOF composites promote rapid catalytic degradation of DMNP CWA simulant with a half-life of less than 5 min.

EXPERIMENTAL SECTION

All reagents were purchased from commercial sources and used without further purification. Zirconium(IV) chloride ($ZrCl_4$, Alfa Aesar, ≥99.5%), 2-aminoterephthalic acid (Acros Organics, 99%), *N*,*N*-dimethylformamide (DMF), deionized water, ethanol, β-cyclodextrin (β-CD, Sigma-Aldrich, ≥97%), cetyltrimethylammonium bromide (CTAB, Sigma-Aldrich, ≥98%), *N*-ethylmorpholine (Sigma-Aldrich, ≥97%), and dimethyl 4-nitrophenyl phosphate (DMNP, Sigma-Aldrich).

Polymeric Fibrous Materials. Nonwoven polypropylene (PP) was received from Nonwovens Cooperative Research Center (NCRC), North Carolina State University. Nonwoven PP fiber mats are 0.30 mm thick, with fiber diameter ranging from 0.6 to 9.0 μm.

Atomic Layer Deposition (ALD). ALD was used to create thin conformal inorganic Al_2O_3, TiO_2, and ZnO coatings on the PP fiber mats. These samples are referred to as PP/Al_2O_3, PP/TiO_2, and PP/ZnO, respectively. The PP/Al_2O_3, TiO_2, and ZnO were deposited directly on the PP. The fiber coating and analysis procedures follow methods developed previously for ALD modification of polymers and textile media.[29]

The ALD Al_2O_3 was deposited onto PP using a lab-made hot-wall viscous-flow vacuum reactor.[21] Deposition pressure was kept at ∼1 Torr, and the temperature was 90 °C. In a general ALD Al_2O_3 cycle, trimethyl aluminum (TMA) was first dosed to the reaction chamber for 1 s, followed with 30 s of N_2 purge between doses. After TMA dose and N_2 purge, deionized water was dosed with another 30 s of N_2 purge. We chose 200 cycles of ALD Al_2O_3 as a standard coating thickness.[21,25,30]

ALD ZnO and TiO_2 were performed in the same lab-made hot-wall viscous-flow vacuum reactor as that used for ALD Al_2O_3. The deposition pressures were both ∼1 Torr, and the temperatures were kept at 90 °C. In an ALD TiO_2 cycle, precursors of both $TiCl_4$ and H_2O were dosed alternately to the reaction chamber for 1 s, with 40 s of N_2 purge between dose steps. We deposited 300 cycles of ALD TiO_2 onto the fiber mats resulting in 20 nm of coating thickness, as determined by ellipsometry on monitor wafers coated simultaneously in the ALD reactor. In an ALD ZnO cycle, the substrate (i.e., PP) was exposed to 2 s of diethyl zinc (DEZ) and 2 s of deionized water alternately, with 60 s of N_2 purge between dose steps. We used 110 cycles of ALD ZnO as a standard coating thickness.[20,31,32]

Synthesis of UiO-66-NH_2 in the Form of Powder. A 20 mL glass scintillation vial was loaded with 0.080 g (0.343 mmol) of $ZrCl_4$ followed by being dissolved in 20 mL of *N*,*N*-dimethylformamide (DMF) and then sonicated for at least 1 min until fully dissolved. After that, 20 μL of deionized water and 0.062 g (0.343 mmol) of 2-aminoterephthalic acid were added to the prepared solution. This as-prepared mixture was heated at 85 °C for 24 h. The resulting solid was then collected by filtering out unreacted precursors and residual DMF using a filtration system. Then the collected solid was rinsed with 80 mL of DMF and ethanol in a sequential manner in the filtration system. Eventually, the final solid was stored under vacuum in a desiccator until being used for the assembly experiment.

Assembly of UiO-66-NH_2 Crystals on Fibers. A total of 0.24 g of as-prepared UiO-66-NH_2 solid was dispersed in 40 mL of DMF and then sonicated for 5 min until fully dispersed (Solution A), and 0.254 g of β-cyclodextrin (β-CD) and 0.04 g of cetyltrimethylammonium bromide (CTAB) were simultaneously dissolved in 40 mL of DMF for an hour to form supramolecular complex (Solution B). Solution for assembly was prepared by slowly pouring solution B to solution A and then keeping the mixture stirred for 30 min.

Assembly of UiO-66-NH_2 crystals onto fiber substrates was performed by immersing PP fiber mats (4 × 2.5 cm) into as-prepared solution with a mild stirring for 20 h at room temperature.

The resulting PP fiber mats with assembled UiO-66-NH_2 crystals were rinsed first with DMF (3 × 80 mL) and then with ethanol (4 × 80 mL). After that, the ultimate products were dried in air for 1 h and stored under vacuum in a desiccator before being used for further characterization.

Hydrolysis of Dimethyl 4-Nitrophenyl Phosphate (DMNP). Hydrolysis for UiO-66-NH_2 powder was implemented at room temperature. UiO-66-NH_2 powder (three respective runs: (1) 1.5 mg, 0.0009 mmol, (2) 2.6 mg, 0.0015 mmol, and (3) 5.6 mg, 0.0032 mmol) was added to an aqueous solution of *N*-ethylmorpholine (1 mL, 0.45 M) in a 1.5 mL Eppendorf vial (room temperature). The resulting mixture was stirred for 30 min until finely dispersing the UiO-66-NH_2. DMNP (∼6.2 mg, 0.025 mmol) was then added to the suspension. Stirring for each reaction was fixed at 1100 rpm.

For periodic monitoring prior to UV/vis measurement, we disposed of a 20 μL aliquot from the reaction mixture and diluting it with an aqueous solution of *N*-ethylmorpholine (10 mL, 0.45 M). Reaction progress was measured by observing the 4-nitrophenoxide absorbance at 407 nm. The solution for background was identical to the reaction solution except for the absence of catalyst.

Hydrolysis for fabric with assembled UiO-66-NH_2 was carried out the same as that for UiO-66-NH_2 powder. Instead of adding the powder sample, we chopped up PP/ZnO + Assembly (two respective runs: (1) 10 mg, 1.8 mg of UiO-66-NH_2 on the fabric, (2) 17.6 mg, 3.2 mg of UiO-66-NH_2 on the fabric; mass fraction of UiO-66-NH_2 on the fabric was about 30.7%) into six pieces and added them into solution for proper hydrolysis reaction with DMNP while being stirred at 1100 rpm.

For monitoring the reaction progress, prior to UV/vis measurement, we disposed of a 20 μL aliquot from the reaction mixture and diluted it with an aqueous solution of *N*-ethylmorpholine (10 mL, 0.45 M). Reaction progress was measured the same way of UiO-66-NH_2 powder. The solution for background was identical to the reaction solution except for the absence of catalyst.

Physical Adhesion Test for UiO-66-NH_2 onto Fabric. The physical adhesion test was conducted by immersing fabric with assembled UiO-66-NH_2 (PP/ZnO + Assembly) in ethanol with vigorous stirring at 500 rpm for 24 h. After the stirring step, the sample was dried in air for 1 h and dried under vacuum at 110 °C overnight. Then, the weight of the sample after vacuum drying was measured and compared with that before the physical adhesion test.

Regeneration of UiO-66-NH_2 (postcatalysis). The slurry of UiO-66-NH_2 after being used for the DMNP hydrolysis experiment was collected and poured onto an Anodisc filter membrane in a glass microanalysis vacuum filter apparatus equipped with a graduated cylinder. Once the sample was dried, 80 mL of deionized water was filtered through the membrane two times. After that, 80 mL of ethanol was passed through the membrane two times. Finally, the UiO-66-NH_2 solid was collected out of the membrane after being fully dried in

DOI: 10.1021/acs.chemmater.7b00949
Chem. Mater. 2017, 29, 4894−4903

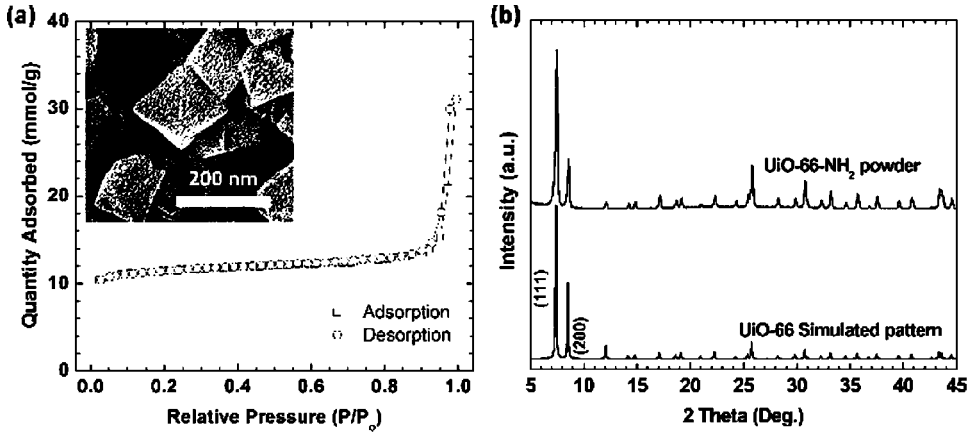

Figure 1. (a) N_2 adsorption (□) and desorption (○) isotherms for the UiO-66-NH_2 powder prepared through solvothermal synthesis at 85 °C for 24 h. Inset indicates the SEM image of UiO-66-NH_2 crystals used for the assembly method. BET surface area of the powder is 956 ± 81 m^2/g with total pore volume of 16 mmol/g calculated at a relative pressure (P/P_0) of 0.95. (b) PXRD data for the UiO-66-NH_2 powder used.

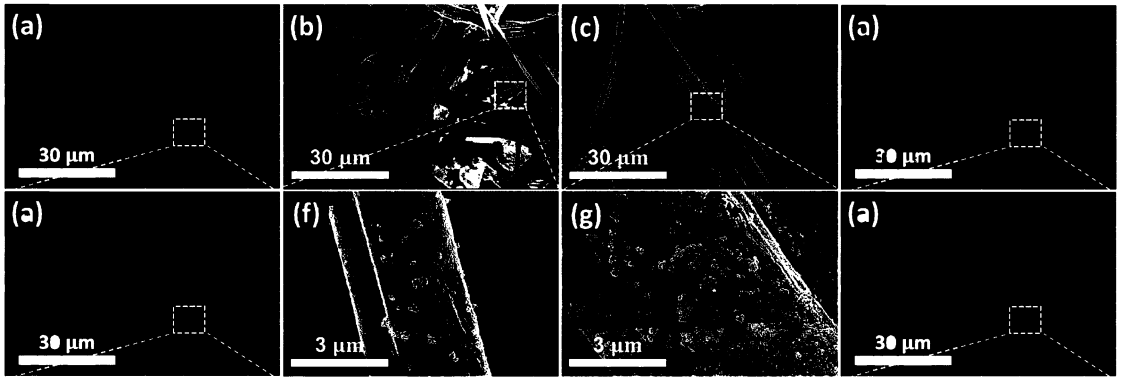

Figure 2. SEM images of samples: (a) PP + Assembly, (b) PP/Al_2O_3 + Assembly, (c) PP/TiO_2 + Assembly, and (d) PP/ZnO + Assembly. Magnified images in dotted circular area of individual images: (e), (f), (g), and (h), respectively. Assembly solution contains as-synthesized UiO-66-NH_2 crystals + β-CD + CTAB.

air and then stored under vacuum in a desiccator for further characterization.

Material Characterization. Scanning electron microscopic (SEM) images were taken using an FEI Verios 460 L field emission SEM. A thin layer of Au−Pd (5−10 nm) was sputter-coated onto all samples before SEM imaging. X-ray diffraction (XRD) was carried out with a Rigaku SmartLab X-ray diffraction tool (Cu Kα X-ray source) for crystalline phase analysis. Both MOF powder (UiO-66-NH_2) and fabric with assembled MOF crystals (PP/ZnO + Assembly) diffraction patterns were also simulated using Mercury 3.0 software and the crystallographic information file from Cambridge Crystallographic Data Centre (CCDC 837796 for UiO-66). A Quantachrome Autosorb-1C surface area and pore size analyzer was used for measuring N_2 isotherm at 77 K. Samples were dried in vacuum (~1 × 10^{-5} Torr) at room temperature for 1 h, at 80 °C for 6 h, 90 °C for 1 h, 100 °C for 1 h, and 110 °C for 12 h in a sequential fashion, before N_2 adsorption measurement. BET surface area was calculated based on the N_2 adsorption data within a relative pressure range of P/P_0 = 0.02−0.08.[33,34] A Thermo Scientific Nicolet 6700 Fourier transform infrared spectrometer was used for analyzing MOF growth on IR silicon wafers. A progressive change in absorbance intensity during hydrolysis reaction was monitored by a Thermo Scientific Evolution 300 UV/vis spectrophotometer.

RESULTS AND DISCUSSION

We prepared UiO-66-NH_2 crystals through solvothermal synthesis as described previously.[35,36] The quality of the as-prepared UiO-66-NH_2 crystals was confirmed via N_2 adsorption isotherms and powder X-ray diffraction (PXRD). In Figure 1, The N_2 adsorption/desorption isotherms show a Brunauer−Emmett−Teller surface area (BET SA) of 956 ± 81 m^2/g and total pore volume of 0.57 cm^3/g, equivalent to 16 mmol/g, and the PXRD results directly matched the simulated UiO-66 pattern, indicating good quality starting MOF powder. To implement the assembly method, we prepared a solution containing UiO-66-NH_2 crystals, β-CD, and CTAB in DMF, along with a similar solution with only the MOF and DMF solvent. For initial experiments, PP substrates with and without ALD coating were immersed in each solution for prolonged periods (up to 20 h) with 500 rpm stirring at ambient temperature. Figure 2 shows SEM images of the uncoated and ALD coated PP after 20 h of assembly in the solution containing β-CD and CTAB. For the uncoated PP, the β-CD/CTAB assembly process leads to homogeneous MOF crystal only in the void regions between the fibers (Figure 2a,e), which we ascribe to crystal entrapment and aggregation during stirring. For the ALD coated PP, we see well-dispersed MOF assembly on Al_2O_3 (Figure 2b,f) and TiO_2 (Figure 2c,d), with somewhat higher surface density on the TiO_2. For the fibers coated with ALD ZnO (Figure 2d,h and Figure S1c), the UiO-66-NH_2 crystals surround and uniformly encase the PP microfibers in a highly packed layer. In some regions, the assembled crystal layer extends between fibers, which was not observed in previous reports for MOFs formed by direct

DOI: 10.1021/acs.chemmater.7b00949
Chem. Mater. 2017, 29, 4894−4903

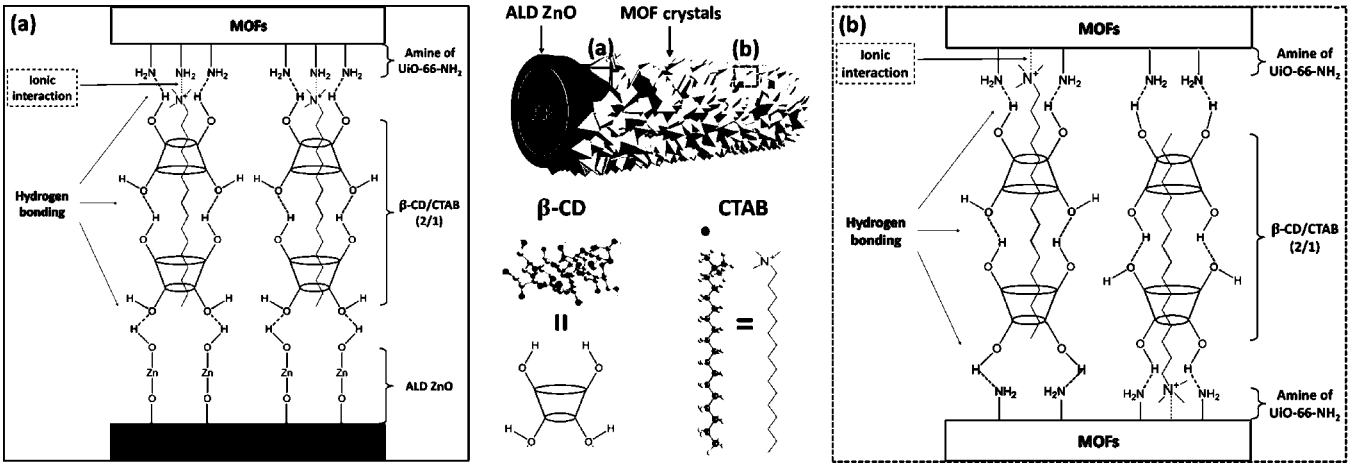

Figure 3. Proposed mechanism of interactions (a) between MOF crystals and ALD ZnO surfaces and (b) MOF crystals themselves by means of β-CD + CTAB structures.

solvothermal synthesis onto fibers.[37] Using ALD-coated PP without the supramolecular complex present, SEM images (Figure S1d) show that, after 20 h in solution, the MOF crystals become trapped and agglomerate within the fabric voids, similar to that in Figure 2a,e for the uncoated PP.[38]

Using the ZnO-coated PP, we also examined assembly using only the individual β-CD or CTAB assembly promoters in the MOF solution. While some MOF loading was observed, the mass uptake with the β-CD or CTAB alone was less than that observed for the combined β-CD + CTAB (Figures S2 and S3). Possible interactions between MOF crystals by means of β-CD + CTAB assembly agents are illustrated in Figure 3. For these tests, the molar ratio of β-CD to CTAB was maintained at the stoichiometric ratio of 2 to 1 to maximize the assembly.[26] We speculate that the ALD ZnO surface deposited on PP fibrous scaffolds can hold hydroxyl groups of β-CD via hydrogen bonding with Zn−OH (Figure 3a). In addition, hydroxyl groups in the outer region of β-CD or cationic heads of CTAB can adhere to electron-rich amine functional groups of the outer MOF surface by means of hydrogen or electrostatic bonding, respectively.[26,28] Therefore, MOF crystals surrounded by the assembly agents (β-CD + CTAB) can be bridged or connected through hydrogen bonding between β-CDs or through van der Waals attractive forces between CTAB tail groups (Figure 3b).

These results show that combining ALD surface preparation with β-CD/CTAB molecular assembly promoters enables well controlled assembly of UiO-66-NH_2 crystals on the surface of flexible fiber webs. Furthermore, we see that the molecular assembly agents or surfactants tend to prevent agglomeration UiO-66-NH_2 crystals in the solution phase, while facilitating assembly on the fiber surface.

Considering these results, we performed more detailed experiments to confirm that the assembled MOFs retained the good crystallinity, surface area, and catalytic activity of the original MOF powders. We also sought to better understand the mechanistic reasons for the observed differences in MOF adhesion on the various ALD metal oxides studied and to characterize the adhesion and stability of the MOFs on the fibers after assembly.

Figure 4a presents the simulated X-ray diffraction patterns of UiO-66-NH_2 powder, the PP substrate, and the MOF-coated PP/ALD fiber mats. The intensity of the primary UiO-66-NH_2

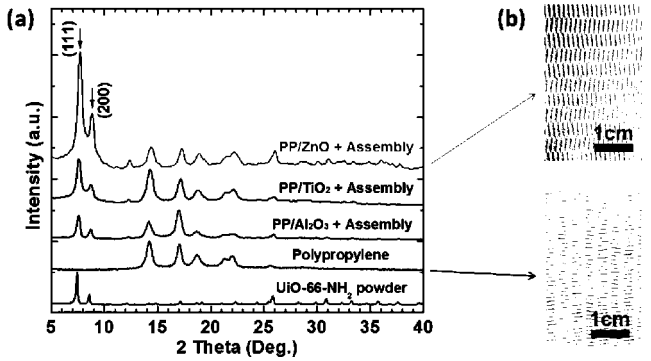

Figure 4. (a) XRD spectra of (from bottom to top) UiO-66-NH_2 powder, polypropylene as a substrate, and samples PP/Al_2O_3 + Assembly, PP/TiO_2 + Assembly, and PP/ZnO + Assembly. (b) Photographs of a virgin PP swatch (bottom) and actual PP/ZnO swatch after "Assembly method" (top). Assembly solution contains as-synthesized UiO-66-NH_2 crystals + β-CD + CTAB.

peaks at 7.2° and 8.3° in 2-theta are strongest for PP/ZnO, consistent with larger mass loading.[10] This sample also shows peaks at 28° to 40° also assigned to UiO-66-NH_2 which are not readily seen in the other experimental patterns. Photographic images of uncoated PP and PP/ZnO fiber mats after MOF assembly are shown in Figure 4b. The yellowish color in the upper image demonstrates the uniform coverage of UiO-66-NH_2 crystals.

Next, we studied mass fraction and overall BET SA of UiO-66-NH_2 crystals assembled onto different ALD layers (Figure 5). In Figure 5a, PP/ZnO + β-CD + CTAB + MOF (referred to as "PP/ZnO + Assembly") shows higher BET SA of 211 m^2/g compared to that of PP/Al_2O_3 + Assembly (79 m^2/g) and PP/TiO_2 + Assembly (90 m^2/g). This is consistent with the result that the highest MOF mass fraction of 30.7% was obtained by PP/ZnO + Assembly. In comparison with overall BET SA of the control samples (i.e., untreated PP fiber mat, 1 m^2/g; PP coated with ALD ZnO, PP/ZnO, 1 m^2/g; and PP + Assembly, 15 m^2/g) the results in Figure 5b depict a large overall BET surface area of 211 m^2/g for the PP/ZnO + Assembly. This value for the BET surface area is slightly less than 287 ± 24 m^2/g expected from the value measured for the pure powder (956 ± 81 m^2/g) and the estimated fraction of MOF mass loading on the fibers. This reduced value may

DOI: 10.1021/acs.chemmater.7b00949
Chem. Mater. 2017, 29, 4894−4903

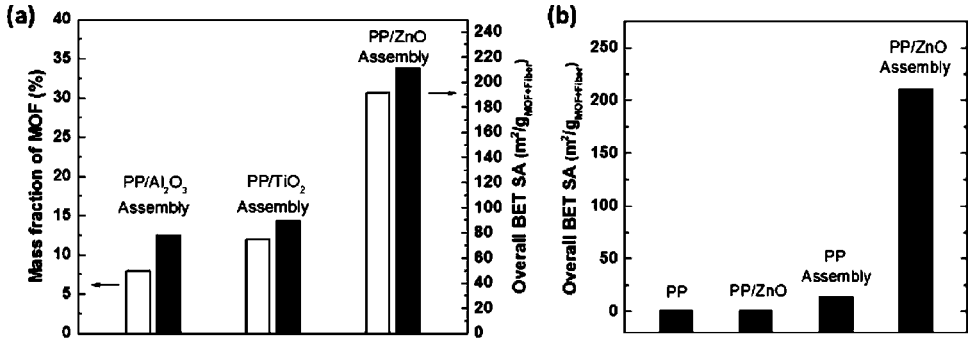

Figure 5. (a) Mass fraction of MOFs on ALD-treated PP + Assembly (left *y*-axis and blank columns) and overall BET surface area for ALD-treated PP + Assembly (right *y*-axis and filled columns). (b) Overall BET surface area for PP, PP/ZnO, PP + Assembly, and PP/ZnO + Assembly. Overall BET surface area means BET surface area of (MOF + Fiber). Assembly solution contains UiO-66-NH_2 + β-CD + CTAB.

reflect uncertainty in the mass loading analysis and/or some partial pore blocking of the surface-anchored MOF crystals by the β-CD + CTAB assembly agents.[39]

The trend in mass loading and surface area with ALD coating composition demonstrates discrepant interactions between the ALD layer and the supramolecular complex (β-CD + CTAB) surrounding the UiO-66-NH_2 crystals. Previous measurements reported the different isoelectric points (IEP) for ALD coatings (i.e., Al_2O_3, TiO_2, or ZnO) and of untreated PP.[31] The surface sites on ZnO and Al_2O_3 (e.g., hydroxyls and bridging oxygens) have predominantly Brønsted basic character, whereas the surfaces of untreated PP and TiO_2 are more acidic. The basic surface sites promote stronger interaction with the assembly agents (β-CD + CTAB), thus promoting MOF attachment. In addition, surface roughness of fiber after the ALD coating may also increase the surface area available for MOF attachment.[20]

As shown in Figure 2a,e and Figure S1, the MOF assembly on the uncoated PP (PP + Assembly) leads to agglomeration of UiO-66-NH_2 crystals within the void regions on the fiber mat substrates. In addition, XRD analysis of MOFs formed within the PP fiber matrix without ALD coating (Figure S4) shows appreciably smaller MOF loading with poor dispersion. We anticipate that these agglomerated crystals do not chemically interact with untreated PP surface, and therefore a smaller amount of MOF crystals is randomly loaded on the fabric. This ultimately leads to relatively small surface area per unit mass (MOF + Fiber). We conclude, therefore, that for the self-assembled MOF on fiber system high overall BET SA requires a procedure that produces both uniform MOF surface distribution and high surface loading.

To test how well the assembled UiO-66-NH_2 crystals are adhered to ALD ZnO-coated PP, we immersed the substrates into ethanol and then vigorously stirred at 500 rpm for 24 h (Figure 6a). From the measured mass change, we found this procedure produced less than 0.1% mass loss (Figure 6b), indicating very strong MOF/surface bonding. As a further test of MOF adhesion, we repeatedly sheared a nylon brush across the UiO-66-NH_2 coated PP substrates. After 30 manual brush strokes, no MOF powder could be visibly detected on the brush or on surrounding surfaces, and as shown in Figure S5, the fabric pieces retained their typical yellow color, indicating good MOF adhesion in the brushed regions.

This strong adhesion of the assembled MOFs on fibers is in distinct contrast to samples prepared without ALD coating or without the β-CD + CTAB complex, where MOFs present on the surface readily fell off under gentle shaking or handling. To examine the MOF assembly mechanism in more detail, we used

(a)

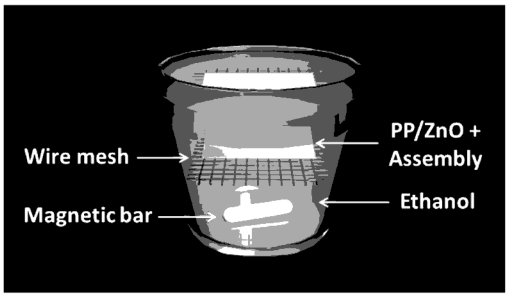

(b)

Sample I.D.	$m/m_{0\ (t=0)}$	$m/m_{0\ (t=24\ h)}$
PP/ZnO + Assembly	1.0	1.0
PP + Assembly	1.0	0.97
UiO–PP/ZnO[⊥]	1.0	0.93

Figure 6. (a) Schematic of the adhesion test during which samples are immersed in ethanol with vigorous stirring at 500 rpm for 24 h and (b) a table revealing comparison of mass change of each sample after the adhesion test. m is mass after completion of the adhesion test, and m_0 is initial mass before the adhesion test. [⊥] For comparison with the conventional solvothermal approach in the attachment of MOF crystals, rather than using "Assembly method", UiO-66-NH_2 is nucleated and grown on PP/ZnO at 85 °C for 24 h.

Fourier transform infrared spectroscopy (FTIR) to investigate changes in the vibrational modes present in each type of prepared sample (Figure 7). Sample substrates were IR transparent silicon with thin native oxide solution coated with CTAB, β-CD, or β-CD + CTAB. Direct IR analysis of the PP fabric was not feasible because of absorbance by the relatively thick polymer fiber. Other silicon samples were coated with thin layers (20 nm) of ALD metal oxides (Al_2O_3, TiO_2, or ZnO) followed by assembly (UiO-66-NH_2 crystals + β-CD + CTAB in DMF) with mild stirring for 20 h. As a further control, we also analyzed silicon wafers coated with ALD TiO_2 followed by solvothermal MOF growth (85 °C for 24 h). All the samples were completely dried in air for 3 h before characterization. This allowed us to carefully trace changes in intrinsic chemical functionalities of the MOF upon assembly and observe differences between assembled and directly grown crystals.

The IR spectra from these samples are shown in Figure 7b,c. The samples with β-CD or β-CD + CTAB show broad ν_{sym}(OH) signals at 3600−3200 cm^{-1} associated with the expected β-CD hydroxyl moieties.[40]

The topmost spectra in Figure 7b,c were collected from the solvothermal MOF films grown on ALD TiO_2 on silicon. The

DOI: 10.1021/acs.chemmater.7b00949
Chem. Mater. 2017, 29, 4894−4903

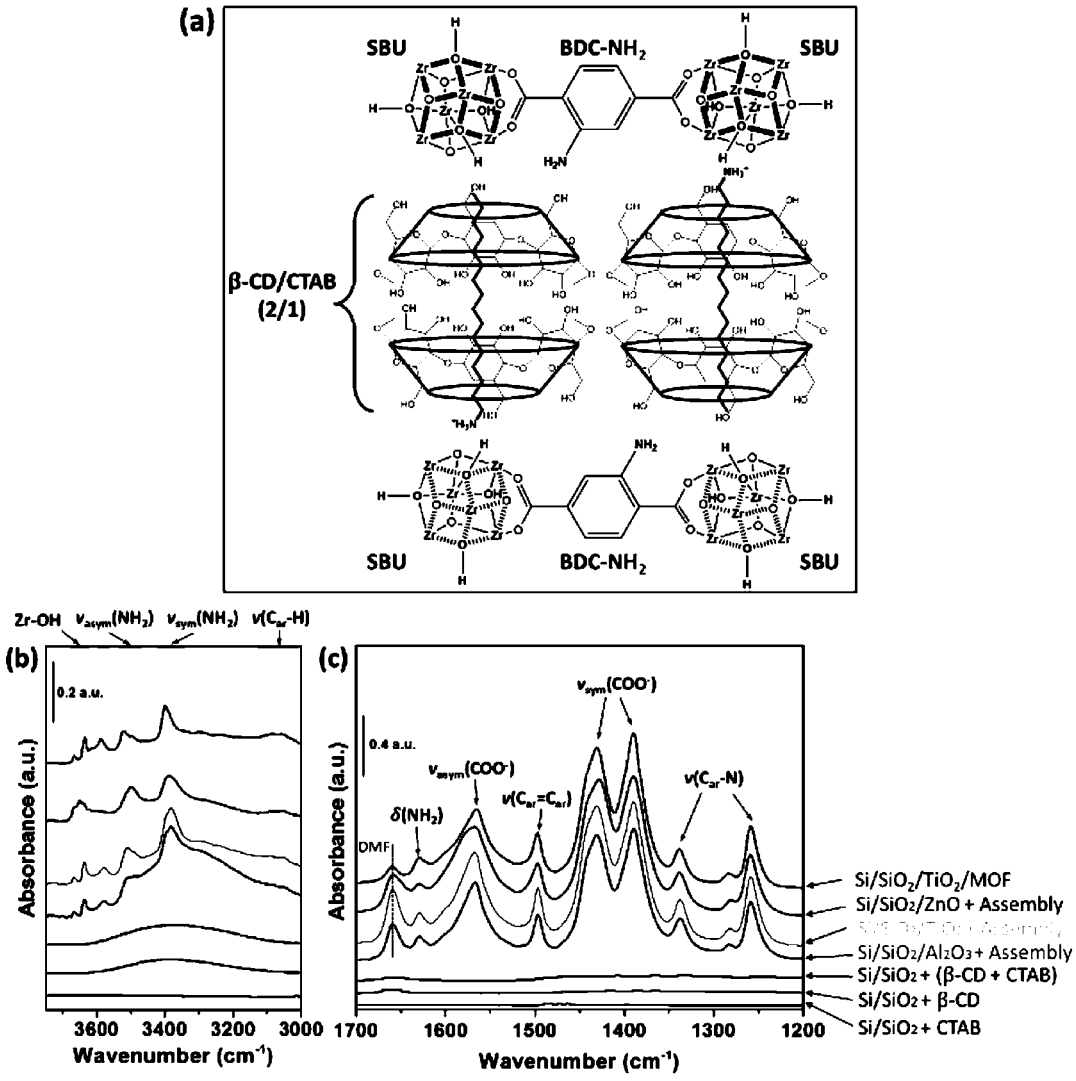

Figure 7. (a) Schematic of expected interactions between MOFs and the supramolecular complex (β-CD + CTAB). (b, c) FTIR spectra of CTAB, β-CD, supramolecular complex (β-CD + CTAB) on Si/SiO_2, UiO-66-NH_2 assembly on ALD-treated (Al_2O_3, TiO_2, or ZnO) Si/SiO_2, and UiO-66-NH_2 grown via solvothermal synthesis (85 °C for 24 h) on $Si/SiO_2/TiO_2$. Note that Si/SiO_2 is used as a background for all FTIR patterns.

spectrum shows OH-related peaks at 3666−3635 cm^{-1} assigned to intrinsic μ_3−OH groups in the $Zr_6O_4(OH)_4$ MOF secondary building unit (SBU) clusters. Peaks associated with the organic aromatic linker (i.e., 2-aminoterephthalic acid) include $\nu_{asym}(NH_2)$ at 3523−3500 cm^{-1}, $\nu_{sym}(NH_2)$ near 3400 cm^{-1}, and aromatic C−H stretches, $\nu(C_{ar}–H)$ at 3100−2850 cm^{-1}.[41] Other MOF-related features in this sample in Figure 7c include $\delta(NH_2)$ at 1629 cm^{-1}, $\nu_{asym}(COO^-)$ at 1566 cm^{-1}, aromatic C=C stretch, $C_{ar}=C_{ar}$ near 1496 cm^{-1}, $\nu_{sym}(COO^-)$ at 1431 and 1390 cm^{-1}, and $\nu(C_{ar}–N)$ at 1338 and 1259 cm^{-1}.[42,43]

Figure 7b,c also shows three additional spectra from MOF films formed by the β-CD/CTAB assembly on ALD TiO_2, ZnO, and Al_2O_3 on silicon. As expected, these spectra show features consistent with the combined MOF and β-CD + CTAB assembly agents. Careful inspection, however, reveals noticeable differences. For example, the intensity of the NH_2 bending mode at 1629 cm^{-1} is reduced for the assembled MOF relative to the grown MOF, particularly for the MOF assembly on ZnO. This change, along with the observable differences in the OH and NH stretching features for the assembled versus grown MOF films, is indicative of the hydrogen bonding and electrostatic interactions that influence the μ_3−OH (on the SBUs), electron-rich amines (on the organic linkers), and terminal OH groups (on β-CD) upon MOF/β-CD/CTAB assembly. The expected structure of the fully assembled MOF on ALD surface is shown schematically in Figure 7a.[44,45] The larger change in the IR for assembly on ZnO is consistent with SEM (Figure 2), XRD (Figure 4), and BET surface area (Figure 5) showing more extensive assembly on ZnO relative to the other metal oxides. One possible difference for assembly on ZnO vs TiO_2 and Al_2O_3 on polypropylene may relate to the role of the ALD precursors in the surface modification of the polymer. On polypropylene, some ALD precursors can readily diffuse into the polymer surface, leading to subsurface metal oxide nucleation and surface roughening. The extent of roughening depends on the polymer, nature of the precursor, ALD reactant dose times, and ALD process temperature.[46,47]

Generally, compared to TiO_2 and Al_2O_3, ZnO ALD tends to produce a roughened surface on PP, whereas on planar silicon, these ALD films will all show smooth surface texture.[48] Therefore, the increased MOF attachment on the ZnO-coated

DOI: 10.1021/acs.chemmater.7b00949
Chem. Mater. 2017, 29, 4894−4903

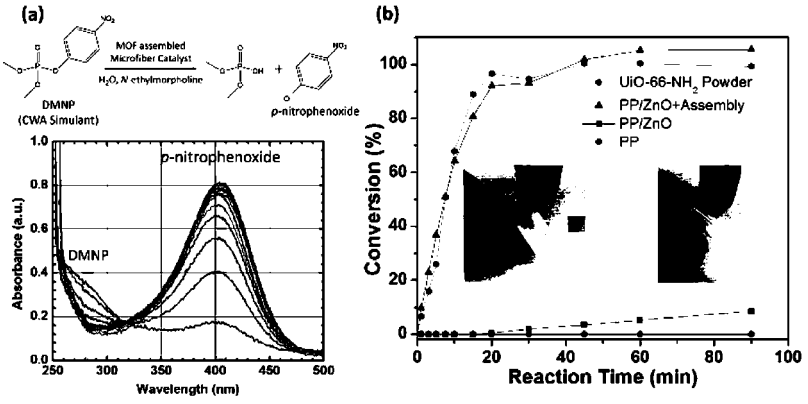

Figure 8. (a) Catalytic hydrolysis reaction for DMNP (top) and UV−vis trace of the hydrolysis of DMNP as a function of time (0−120 min) using PP/ZnO + Assembly fiber mats (bottom). (b) Conversion profiles for the hydrolysis of DMNP in the presence of PP, PP/ZnO, PP/ZnO + Assembly, and UiO-66-NH_2 powder at room temperature as a function of time. Inset shows transparent color of solution before hydrolysis reaction starts remarkably changed into yellowish one after the reaction completes. *UiO-66-NH_2 powder used is collected from remnants of the assembly solution. The slight drop in the data at ∼30 min is within the statistical uncertainty of the results.

PP may be also associated with preferred attachment on roughened polymer substrates.

To evaluate the functional performance of the fiber-surface assembled UiO-66-NH_2 MOF crystals, we performed experiments using assembled UiO-66-NH_2 crystals as catalytic agents for hydrolysis of chemical warfare agent simulants.[37,49,50] Here, we used DMNP and examined the rate of the phosphate ester bond hydrolysis to simulate hydrolysis of GB (Sarin) or GD (Soman) nerve agents that each contain a labile P−F bond.[51] Katz et al. have recently found that the DMNP hydrolysis rate using UiO-66-NH_2 is approximately 20 times that of UiO-66.[52] This noticeable enhancement was probably by the amino moiety functioning as a Brønsted-base in UiO-66-NH_2, improving proton transfer during the hydrolysis. Figure 8a shows a schematic of the hydrolysis of DMNP by MOF-based catalyst (left) and periodic monitoring (right) of the hydrolysis reaction using UV−vis measurements. As the reaction progresses, the intensity at 407 nm becomes enhanced due to emergence of the 4-nitrophenoxide hydrolysis product. Conversion profiles for DMNP hydrolysis in the presence of untreated PP, PP/ZnO, PP/ZnO + Assembly, and UiO-66-NH_2 MOF powder are plotted, respectively. As shown in Figure 8b and Table 1, for untreated PP microfibers, the DMNP destruction rate is negligible with the estimated half-life of around 6 days. With ALD ZnO layers on PP microfibers (PP/ZnO), it lowers the half-life to less than 20 h (Figure S6). This shows consistency that metal oxides like TiO_2 or ZnO can function as catalysts for degrading CWAs or their simulants.[53,54] The DMNP hydrolysis reaction rates are much faster with PP/ZnO + Assembly ($m_{(MOF+Fabric)}$ = 10 mg) fabric and (m_{MOF} = 2.6 mg) UiO-66-NH_2 powder with the half-life of 6.5 min for both. The kinetic traces and half-lives of hydrolysis of DMNP using the fabric and powder samples are close to each other. We believe this observation is reasonable considering that mass fraction of UiO-66-NH_2 on the fabric (PP/ZnO + Assembly) was around 30.7%. Therefore, it is sensible to regard the amount of MOFs on the fabric as about 3.1 mg, which is a similar amount of MOFs in the powder sample (m_{MOF} = 2.6 mg). Furthermore, the rates for DMNP degradation are similar to those recently reported for UiO-66-NH_2 formed on ALD-coated polymer fibers via direct solvothermal synthesis.[36] As for the hydrolysis reactions catalyzed with the fabric samples, we cut one piece of fabric into several pieces to well disperse in the reacting solution. As a control experiment, we kept the total amount of sample (MOF + fiber) fixed and varied the extent of fabric cutting used to prepare the samples for kinetic analysis. Results in Figure S7 show we obtained the same DMNP degradation rate using either a single fabric piece or a sample cut into small pieces, confirming that sample cutting did not influence measured reaction kinetics.

Table 1. Material Properties and Catalytic Performance of Degrading a CWA Simulant, DMNP[a]

material	amount of catalyst [μmol]	MOF wt %	k [min^{-1}]	$t_{1/2}$ [min]	TOF (s^{-1})
Powder					
UiO-66-NH_2 (l.5 mg)	0.9	100	0.019	36.5	0.0063
UiO-66-NH_2 (2.6 mg)	1.5	100	0.111	6.5	0.021
UiO-66-NH_2 (5.6 mg)	3.3	100	0.301	2.5	0.025
Fabric					
untreated PP (14.0 mg)	0	0	7.98×10^{-5}	8690	-
PP/ZnO (14.0 mg)	0	0	5.87×10^{-4}	1182	-
PP/ZnO + Assembly (10.0 mg]	1.8[b]	30.7	0.105	6.5	0.018
PP/ZnO + Assembly (17.6 mg)	3.2[b]	30.7	0.245	2.8	0.023

[a]UiO-66-NH_2 powder used was collected from remnants of assembly solution. Turn over frequency (TOF) was calculated per Zr_6 cluster at $t_{1/2}$. [b]Amount of catalyst for fabric samples is corrected based on the actual mass fraction of UiO-66-NH_2 assembled on PP/ZnO, which is about 30.7% as calculated in Figure 5a.

In another set of experiments, we varied the catalyst loading and found that the initial $t_{1/2}$ values are diminished as the amounts of the catalyst loading are increased (Figure S8 and Table 1). These results are analogous to those with UiO-67 derivatives previously reported.[52] We also identified that such kinetic traces with fabric (PP/ZnO + Assembly) samples showed similar propensity (Figure S9 and Table 1).

Concerning verified high mechanical and hydrostability of UiO-66-NH_2, XRD and SEM confirmed that UiO-66-NH_2 is

DOI: 10.1021/acs.chemmater.7b00949
Chem. Mater. 2017, 29, 4894−4903

fairly intact under our hydrolysis condition (Figure S10). Moreover, we confirmed that the microstructure of the UiO-66-NH_2 is retained after assembly, as determined by overall BET SA of the MOFs. The surface area of 817 m^2/g after assembly is very close to 956 ± 81 m^2/g measured for similarly prepared UiO-66-NH_2 crystals. This difference probably reflects the extra mass of the supramolecular complex or perhaps partial blocking of the accessibly MOF pores.[39] Even so, the BET surface area remains similar to values of ca. 830 m^2/g reported for some pristine UiO-66-NH_2 powders.[22] Considering all results collectively, chemical assembly of UiO-66-NH_2 on polymer fabric is a viable means to create MOF-cloths for chemical hydrolysis agents simulated by DMNP with half-life less than 5 min.

CONCLUSIONS

The results described here clearly demonstrate that combining ALD surface modification with solution-based β-CD + CTAB supramolecular complex adhesion promotor allows assembly of high density, robust, and functionally active MOF crystal coatings on fiber-based substrates. The assembly approach is summarized in Scheme 1. The ALD layer provides a chemically functional attachment layer for the supramolecular β-CD + CTAB complex, and the complex acts as an assembly agent to well disperse UiO-66-NH_2 crystals and allow them to assemble into dense coatings onto the ALD layers via electrostatic and hydrogen bonding interactions. We find that the extent of MOF loading depends on the composition of the metal oxide ALD coating, with a larger extent of loading on ZnO vs Al_2O_3 or TiO_2. Infrared analysis confirms that assembled layers contain β-CD, CTAB, and MOF crystals, and analysis of the IR results suggests that surface composition as well as fiber surface roughness may be factors in the extent of MOF loading.

We also verified that the crystals assembled on PP fibrous mats retain their effectiveness for rapid catalytic degradation of hazardous chemical simulants, with rates in line with those observed for the same reactions on UiO-66-NH_2 MOFs in free-powder form. The results clearly show that chemically assembling a relatively small amount of MOF crystals on a fiber surface can be beneficial to overcome difficulties in deployment of MOF powders. Moreover, the assembly process proceeds readily at room temperature and therefore can be considered for extending to a wide range of substrate materials at large scale.

Scheme 1. Comparison of "Assembly Method" at Ambient Temperature between Untreated Polypropylene (PP) and ALD-Treated PP[a]

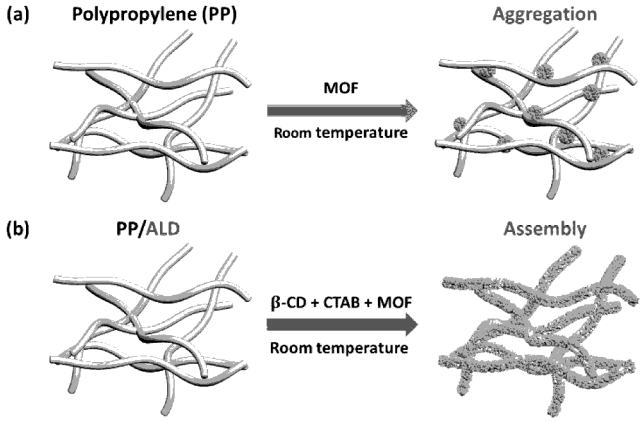

[a]Solution for assembly contains presynthesized UiO-66-NH_2 crystals and the supramolecular complex (β-cyclodextrin (β-CD) + cetyltrimethylammonium bromide (CTAB)).

ASSOCIATED CONTENT

Supporting Information

The Supporting Information is available free of charge on the ACS Publications website at DOI: 10.1021/acs.chemmater.7b00949.

Additional information pertaining to SEM, MOF adhesion tests, kinetic studies, and XRD (PDF)

AUTHOR INFORMATION

Corresponding Author

*(G.N.P.) E-mail: parsons@ncsu.edu.

ORCID

Dennis T. Lee: 0000-0002-1976-2852

Gregory W. Peterson: 0000-0003-3467-5295

Author Contributions

The manuscript was written through contributions of all authors. All authors have given approval to the final version of the manuscript.

Notes

The authors declare no competing financial interest.

ACKNOWLEDGMENTS

The authors acknowledge support from ECBC (Grant W911SR-07-C-0075) and the Joint Science and Technology Office (Army Research Office Grant W911NF-13-1-0173). We acknowledge the excess of the Analytical Instrumentation Facility (AIF) at North Carolina State University, supported by the State of North Carolina and National Science Foundation.

REFERENCES

(1) Horike, S.; Shimomura, S.; Kitagawa, S. Soft porous crystals. *Nat. Chem.* **2009**, *1*, 695−704.

(2) Howarth, A. J.; Liu, Y. Y.; Li, P.; Li, Z. Y.; Wang, T. C.; Hupp, J.; Farha, O. K. Chemical, thermal and mechanical stabilities of metal-organic frameworks. *Nat. Mater. Rev.* **2016**, *1*, 15018.

(3) Mason, J. A.; Veenstra, M.; Long, J. R. Evaluating metal-organic frameworks for natural gas storage. *Chem. Sci.* **2014**, *5*, 32−51.

(4) Lee, J.; Farha, O. K.; Roberts, J.; Scheidt, K. A.; Nguyen, S. T.; Hupp, J. T. Metal-organic framework materials as catalysts. *Chem. Soc. Rev.* **2009**, *38*, 1450−1459.

(5) So, M. C.; Wiederrecht, G. P.; Mondloch, J. E.; Hupp, J. T.; Farha, O. K. Metal-organic framework materials for light-harvesting and energy transfer. *Chem. Commun.* **2015**, *51*, 3501−3510.

(6) Howarth, A. J.; Wang, T. C.; Al-Juaid, S. S.; Aziz, S. G.; Hupp, J. T.; Farha, O. K. Efficient extraction of sulfate from water using a Zr-metal-organic framework. *Dalton Trans.* **2016**, *45*, 93−97.

(7) DeCoste, J. B.; Peterson, G. W. Metal-Organic Frameworks for Air Purification of Toxic Chemicals. *Chem. Rev.* **2014**, *114*, 5695−5727.

(8) Peterson, G. W.; Moon, S. Y.; Wagner, G. W.; Hall, M. G.; DeCoste, J. B.; Hupp, J. T.; Farha, O. K. Tailoring the Pore Size and Functionality of UiO-Type Metal-Organic Frameworks for Optimal Nerve Agent Destruction. *Inorg. Chem.* **2015**, *54*, 9684−9686.

(9) Li, J. R.; Kuppler, R. J.; Zhou, H. C. Selective gas adsorption and separation in metal-organic frameworks. *Chem. Soc. Rev.* **2009**, *38*, 1477−1504.

DOI: 10.1021/acs.chemmater.7b00949
Chem. Mater. 2017, 29, 4894−4903

(10) Pinto, M. L.; Dias, S.; Pires, J. Composite MOF Foams: The Example of UiO-66/Polyurethane. *ACS Appl. Mater. Interfaces* **2013**, *5*, 2360−2363.
(11) Liu, C.; Wu, Y. N.; Morlay, C.; Gu, Y. F.; Gebremariam, B.; Yuan, X.; Li, F. T. General Deposition of Metal-Organic Frameworks on Highly Adaptive Organic-Inorganic Hybrid Electrospun Fibrous Substrates. *ACS Appl. Mater. Interfaces* **2016**, *8*, 2552−2561.
(12) Fan, L. L.; Xue, M.; Kang, Z. X.; Li, H.; Qiu, S. L. Electrospinning technology applied in zeolitic imidazolate framework membrane synthesis. *J. Mater. Chem.* **2012**, *22*, 25272−25276.
(13) Li, Y. B.; Wee, L. H.; Volodin, A.; Martens, J. A.; Vankelecom, I. F. J. Polymer supported ZIF-8 membranes prepared via an interfacial synthesis method. *Chem. Commun.* **2015**, *51*, 918−920.
(14) Li, S.; Huo, F. Metal-organic framework composites: from fundamentals to applications. *Nanoscale* **2015**, *7*, 7482−7501.
(15) Armstrong, M. R.; Arredondo, K. Y. Y.; Liu, C. Y.; Stevens, J. E.; Mayhob, A.; Shan, B. H.; Senthilnathan, S.; Balzer, C. J.; Mu, B. UiO-66 MOF and Poly(vinyl cinnamate) Nanofiber Composite Membranes Synthesized by a Facile Three-Stage Process. *Ind. Eng. Chem. Res.* **2015**, *54*, 12386−12392.
(16) Guo, H.; Zhu, G.; Hewitt, I. J.; Qiu, S. Twin Copper Source" Growth of Metal−Organic Framework Membrane: Cu3(BTC)2 with High Permeability and Selectivity for Recycling H2. *J. Am. Chem. Soc.* **2009**, *131*, 1646−1647.
(17) So, M. C.; Jin, S.; Son, H. J.; Wiederrecht, G. P.; Farha, O. K.; Hupp, J. T. Layer-by-Layer Fabrication of Oriented Porous Thin Films Based on Porphyrin-Containing Metal-Organic Frameworks. *J. Am. Chem. Soc.* **2013**, *135*, 15698−15701.
(18) Yao, J. F.; Dong, D. H.; Li, D.; He, L.; Xu, G. S.; Wang, H. T. Contra-diffusion synthesis of ZIF-8 films on a polymer substrate. *Chem. Commun.* **2011**, *47*, 2559−2561.
(19) Yoo, Y.; Jeong, H. K. Rapid fabrication of metal organic framework thin films using microwave-induced thermal deposition. *Chem. Commun.* **2008**, 2441−2443.
(20) Zhao, J.; Losego, M. D.; Lemaire, P. C.; Williams, P. S.; Gong, B.; Atanasov, S. E.; Blevins, T. M.; Oldham, C. J.; Walls, H. J.; Shepherd, S. D.; Browe, M. A.; Peterson, G. W.; Parsons, G. N. Highly Adsorptive, MOF-Functionalized Nonwoven Fiber Mats for Hazardous Gas Capture Enabled by Atomic Layer Deposition. *Adv. Mater. Interfaces* **2014**, *1*, 1400040.
(21) Zhao, J.; Gong, B.; Nunn, W. T.; Lemaire, P. C.; Stevens, E. C.; Sidi, F. I.; Williams, P. S.; Oldham, C. J.; Walls, H. J.; Shepherd, S. D.; Browe, M. A.; Peterson, G. W.; Losego, M. D.; Parsons, G. N. Conformal and highly adsorptive metal-organic framework thin films via layer-by-layer growth on ALD-coated fiber mats. *J. Mater. Chem. A* **2015**, *3*, 1458−1464.
(22) Katz, M. J.; Brown, Z. J.; Colon, Y. J.; Siu, P. W.; Scheidt, K. A.; Snurr, R. Q.; Hupp, J. T.; Farha, O. K. A facile synthesis of UiO-66, UiO-67 and their derivatives. *Chem. Commun.* **2013**, *49*, 9449−9451.
(23) Mondloch, J. E.; Katz, M. J.; Isley, W. C., III; Ghosh, P.; Liao, P. L.; Bury, W.; Wagner, G.; Hall, M. G.; DeCoste, J. B.; Peterson, G. W.; Snurr, R. Q.; Cramer, C. J.; Hupp, J. T.; Farha, O. K. Destruction of chemical warfare agents using metal-organic frameworks. *Nat. Mater.* **2015**, *14*, 512−516.
(24) Chen, Q.; He, Q. Q.; Lv, M. M.; Xu, Y. L.; Yang, H. B.; Liu, X. T.; Wei, F. Y. Selective adsorption of cationic dyes by UiO-66-NH2. *Appl. Surf. Sci.* **2015**, *327*, 77−85.
(25) Hyde, G. K.; Scarel, G.; Spagnola, J. C.; Peng, Q.; Lee, K.; Gong, B.; Roberts, K. G.; Roth, K. M.; Hanson, C. A.; Devine, C. K.; Stewart, S. M.; Hojo, D.; Na, J. S.; Jur, J. S.; Parsons, G. N. Atomic Layer Deposition and Abrupt Wetting Transitions on Nonwoven Polypropylene and Woven Cotton Fabrics. *Langmuir* **2010**, *26*, 2550−2558.
(26) Kumar, P.; Kim, W. D.; Lee, S.; Lee, D. T.; Lee, K.; Lee, D. C. Surface energy-driven growth of crystalline PbS octahedra and dendrites in the presence of cyclodextrin-surfactant supramolecular complexes. *J. Nanopart. Res.* **2015**, *17*, 108.
(27) Depalo, N.; Comparelli, R.; Striccoli, M.; Curri, M. L.; Fini, P.; Giotta, L.; Agostiano, A. alpha-cyclodextrin functionalized CdS nanocrystals for fabrication of 2/3 D assemblies. *J. Phys. Chem. B* **2006**, *110*, 17388−17399.
(28) Huang, T.; Meng, F.; Qi, L. M. Controlled Synthesis of Dendritic Gold Nanostructures Assisted by Supramolecular Complexes of Surfactant with Cyclodextrin. *Langmuir* **2010**, *26*, 7582−7589.
(29) Brozena, A. H.; Oldham, C. J.; Parsons, G. N. Atomic layer deposition on polymer fibers and fabrics for multifunctional and electronic textiles. *J. Vac. Sci. Technol., A* **2016**, *34*, 010801.
(30) Jur, J. S.; Spagnola, J. C.; Lee, K.; Gong, B.; Peng, Q.; Parsons, G. N. Temperature-Dependent Subsurface Growth during Atomic Layer Deposition on Polypropylene and Cellulose Fibers. *Langmuir* **2010**, *26*, 8239−8244.
(31) Lemaire, P. C.; Zhao, J. J.; Williams, P. S.; Walls, H. J.; Shepherd, S. D.; Losego, M. D.; Peterson, G. W.; Parsons, G. N. Copper Benzenetricarboxylate Metal-Organic Framework Nucleation Mechanisms on Metal Oxide Powders and Thin Films formed by Atomic Layer Deposition. *ACS Appl. Mater. Interfaces* **2016**, *8*, 9514−9522.
(32) Zhao, J.; Nunn, W. T.; Lemaire, P. C.; Lin, Y.; Dickey, M. D.; Oldham, C. J.; Walls, H. J.; Peterson, G. W.; Losego, M. D.; Parsons, G. N. Facile Conversion of Hydroxy Double Salts to Metal−Organic Frameworks Using Metal Oxide Particles and Atomic Layer Deposition Thin-Film Templates. *J. Am. Chem. Soc.* **2015**, *137*, 13756−13759.
(33) Wong-Foy, A. G.; Matzger, A. J.; Yaghi, O. M. Exceptional H-2 saturation uptake in microporous metal-organic frameworks. *J. Am. Chem. Soc.* **2006**, *128*, 3494−3495.
(34) Walton, K. S.; Snurr, R. Q. Applicability of the BET Method for Determining Surface Areas of Microporous Metal−Organic Frameworks. *J. Am. Chem. Soc.* **2007**, *129*, 8552−8556.
(35) Schaate, A.; Roy, P.; Godt, A.; Lippke, J.; Waltz, F.; Wiebcke, M.; Behrens, P. Modulated Synthesis of Zr-Based Metal-Organic Frameworks: From Nano to Single Crystals. *Chem. - Eur. J.* **2011**, *17*, 6643−6651.
(36) Zhao, J.; Lee, D. T.; Yaga, R. W.; Hall, M. G.; Barton, H. F.; Woodward, I. R.; Oldham, C. J.; Walls, H. J.; Peterson, G. W.; Parsons, G. N. Ultra-Fast Degradation of Chemical Warfare Agents Using MOF-Nanofiber Kebabs. *Angew. Chem., Int. Ed.* **2016**, *55*, 13224−13228.
(37) Lopez-Maya, E.; Montoro, C.; Rodriguez-Albelo, L. M.; Cervantes, S. D. A.; Lozano-Perez, A. A.; Cenis, J. L.; Barea, E.; Navarro, J. A. R. Textile/Metal-Organic-Framework Composites as Self-Detoxifying Filters for Chemical-Warfare Agents. *Angew. Chem., Int. Ed.* **2015**, *54*, 6790−6794.
(38) Wang, H.; Wu, Y. M.; Bai, Y. S.; Zhou, W.; An, Y. R.; Li, J. H.; Guo, L. The self-assembly of porous microspheres of tin dioxide octahedral nanoparticles for high performance lithium ion battery anode materials. *J. Mater. Chem.* **2011**, *21*, 10189−10194.
(39) Qiu, L. G.; Xu, T.; Li, Z. Q.; Wang, W.; Wu, Y.; Jiang, X.; Tian, X. Y.; Zhang, L. D. Hierarchically Micro- and Mesoporous Metal-Organic Frameworks with Tunable Porosity. *Angew. Chem., Int. Ed.* **2008**, *47*, 9487−9491.
(40) Shokuhfar, A.; Afghahi, S. S. S. The heating effect of iron-cobalt magnetic nanofluids in an alternating magnetic field: application in magnetic hyperthermia treatment. *Nanoscale Res. Lett.* **2013**, *8*, 540.
(41) Peterson, G. W.; McEntee, M.; Harris, C. R.; Klevitch, A. D.; Fountain, A. W.; Soliz, J. R.; Balboa, A.; Hauser, A. J. Detection of an explosive simulant via electrical impedance spectroscopy utilizing the UiO-66-NH2 metal-organic framework. *Dalton Trans.* **2016**, *45*, 17113−17116.
(42) Kandiah, M.; Usseglio, S.; Svelle, S.; Olsbye, U.; Lillerud, K. P.; Tilset, M. Post-synthetic modification of the metal-organic framework compound UiO-66. *J. Mater. Chem.* **2010**, *20*, 9848−9851.
(43) Cavka, J. H.; Jakobsen, S.; Olsbye, U.; Guillou, N.; Lamberti, C.; Bordiga, S.; Lillerud, K. P. A new zirconium inorganic building brick forming metal organic frameworks with exceptional stability. *J. Am. Chem. Soc.* **2008**, *130*, 13850−13851.

DOI: 10.1021/acs.chemmater.7b00949
Chem. Mater. 2017, 29, 4894−4903

(44) Lv, G. R.; Liu, J. M.; Xiong, Z. H.; Zhang, Z. H.; Guan, Z. Y. Selectivity Adsorptive Mechanism of Different Nitrophenols on UIO-66 and UIO-66-NH2 in Aqueous Solution. *J. Chem. Eng. Data* **2016**, *61*, 3868−3876.
(45) Howarth, A. J.; Liu, Y. Y.; Hupp, J. T.; Farha, O. K. Metal-organic frameworks for applications in remediation of oxyanion/cation-contaminated water. *CrystEngComm* **2015**, *17*, 7245−7253.
(46) Spagnola, J. C.; Gong, B.; Arvidson, S. A.; Jur, J. S.; Khan, S. A.; Parsons, G. N. Surface and sub-surface reactions during low temperature aluminium oxide atomic layer deposition on fiber-forming polymers. *J. Mater. Chem.* **2010**, *20*, 4213−4222.
(47) Sweet, W. J.; Parsons, G. N. In Situ Conductance Analysis of Zinc Oxide Nucleation and Coalescence during Atomic Layer Deposition on Metal Oxides and Polymers. *Langmuir* **2015**, *31*, 7274−7282.
(48) Sweet, W. J.; Jur, J. S.; Parsons, G. N. Bi-layer Al2O3/ZnO atomic layer deposition for controllable conductive coatings on polypropylene nonwoven fiber mats. *J. Appl. Phys.* **2013**, *113*, 194303.
(49) Moon, S. Y.; Liu, Y. Y.; Hupp, J. T.; Farha, O. K. Instantaneous Hydrolysis of Nerve-Agent Simulants with a Six-Connected Zirconium-Based Metal-Organic Framework. *Angew. Chem., Int. Ed.* **2015**, *54*, 6795−6799.
(50) Wang, S.; Bromberg, L.; Schreuder-Gibson, H.; Hatton, T. A. Organophophorous Ester Degradation by Chromium(III) Terephthalate Metal-Organic Framework (MIL-101) Chelated to N,N-Dimethylaminopyridine and Related Aminopyridines. *ACS Appl. Mater. Interfaces* **2013**, *5*, 1269−1278.
(51) Katz, M. J.; Mondloch, J. E.; Totten, R. K.; Park, J. K.; Nguyen, S. T.; Farha, O. K.; Hupp, J. T. Simple and Compelling Biomimetic Metal-Organic Framework Catalyst for the Degradation of Nerve Agent Simulants. *Angew. Chem., Int. Ed.* **2014**, *53*, 497−501.
(52) Katz, M. J.; Moon, S. Y.; Mondloch, J. E.; Beyzavi, M. H.; Stephenson, C. J.; Hupp, J. T.; Farha, O. K. Exploiting parameter space in MOFs: a 20-fold enhancement of phosphate-ester hydrolysis with UiO-66-NH2. *Chem. Sci.* **2015**, *6*, 2286−2291.
(53) Wagner, G. W.; Chen, Q.; Wu, Y. Reactions of VX, GD, and HD with nanotubular titania. *J. Phys. Chem. C* **2008**, *112*, 11901−11906.
(54) Bisio, C.; Carniato, F.; Palumbo, C.; Safronyuk, S. L.; Starodub, M. F.; Katsev, A. M.; Marchese, L.; Guidotti, M. Nanosized inorganic metal oxides as heterogeneous catalysts for the degradation of chemical warfare agents. *Catal. Today* **2016**, *277*, 192−199.

DOI: 10.1021/acs.chemmater.7b00949
Chem. Mater. 2017, 29, 4894−4903